NUMERICAL AND EXPERIMENTAL MODELING OF TURBULENT FLOWS IN FURNACE CHAMBERS

S. V. Alekseenko, V. D. Goryachev,
I. N. Gusev, V. M. Eroshenko,
and V. B. Rabovskii

UDC 532.517.4:662.9

Results are presented from an experimental and numerical modeling of two-dimensonal turbulent flows in furnace chambers. The article follows the evolution of the flow patterns with a change in the configuration of the chamber. The range of validity of the study results are discussed.

The combustion of organic fuels in chamber-type furnaces is widely used in power generation in this country. Environmental requirements and high fuel costs are forcing furnace designers to seek continued improvements in power-producing equipment. Progress in this area hinges to a considerable extent on a proper understanding of the corresponding physical mechanisms.

Modeling processes in the furnaces of power-plant boilers is an extremely complex problem due to the need to account for a large number of simultaneously acting and interrelated factors. Physical modeling is made even more difficult in this case when the capacity of the boiler and, thus, its linear dimensions are being increased from previous designs. As was shown, the agreement that can be obtained between the similarity criteria for the model and the actual object in physical modeling may only be approximate — even for individual groups of criteria. In addition, several parameters generally are not amenable to measurement. For example, the velocity distribution in pulverized-coal flames cannot be measured by current experimental methods because of slag encrustation of the probes. As a result of this situation, mathematical modeling techniques have assumed more importance in recent years. It is reasoned that studies conducted on actual models can be partially replaced or supplemented by calculations. An adequate mathematical model makes it possible to significantly advance our understnding of the physical aspects of a given phenomenon and, instead of using discrete local parameters of the object, to represent all of its properties and proceed readily from one possible design to another.

A mathematical model of the processes occurring in a furnace should include aerodynamics, convective and radiative heat transfer, and combustion processes. Thus, modeling aerodynamics under isothermal conditions is an important step in the construction of a general model. Previous studies conducted in this area have as a rule been concerned with axisymmetric flows [2]. Such flows can be described within the framework of a two-dimensional approach. Calculations have also recently been performed for three-dimensional turbulent flows [3-6], although they have been mainly of an illustrative nature due to the inherent complexity of this problem. It should be noted that the completeness of the modeling is constrained by the capabilities of modern computers. This limiting factor makes it impossible to achieve the level of detail that can be attained when modeling simpler flows. There are also several difficulties related directly to the computing process, such as the large difference in the dimensions of the burners and the furnace as a whole and the presence of numerical (artificial) viscosity. Ignoring these aspects of the problem may make all attempts to improve the model of turbulent flow fruitless.

The present study is devoted to a theoretical and experimental investigation of isothermal flows in different types of furnace chambers. The numerical method used is based on differential equations for the velocity components, augmented by a $k-\varepsilon$ model of a fully developed turbulent flow.

G. M. Krizhizhanovskii State Scientific-Research Energy Institute, Moscow. Translated from Inzhenerno-Fizicheskii Zhurnal, Vol. 59, No. 6, pp. 948-956, December, 1990. Original article submitted June 28, 1989.

0022-0841/90/5906-1545$12.50

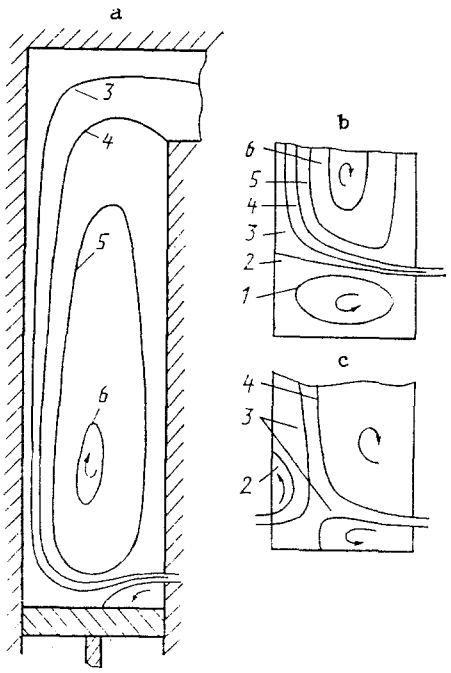

Fig. 1. Streamlines normalized for the total discharge (a, b — unilateral delivery; c — bilateral delivery: a, c — H = 0.03 m; b — 0.065): 1 — F = −0.5; 2 — 0; 3 — 0.5; 4 — 1; 5 — 1.5; 6 — 2.

The application package that was developed for the study is oriented toward furnace chambers possessing translational symmetry along one of the coordinates. Flow in such chambers is of a two-dimensional nature. Spatial effects are insignificant and are determined by the degree of influence of the front and rear walls. Another factor which acts to distort the two-dimensional character of the flow field as a whole is the noncoincidence of the scales and geometries of the burners and the furnace chamber. Fuel is usually admitted through a large number of axisymmetric burners, while actual combustion takes place in rectangular chambers. However, the structure of the flow in the immediate vicinity of the burners does not have a large effect on the overall pattern of the aerodynamic fields. At the current stage of investigation, this makes it possible to replace the burner zone by a single nozzle. The velocity at the outlet of the nozzle should be chosen so as to conform to the consumption of the fuel—air mixture. The range of validity of such a simplification is discussed below.

Experiments were conducted on a closed-type unit with a changeable working section. The hydrodynamic loop included a 200-liter tank, centrifugal pump, connecting pipes, and control valves. Figure 1 shows the overall appearance of the working section — a rectangular channel 700 mm high, 162 mm wide, and 86 mm deep. With certain simplifications, this section simulated the furnace chamber we wished to study. The working fluid (distilled water under normal conditions) was delivered through slotted nozzles with a width of 9 mm. The possibility of design changes was provided for through the use of a movable bottom. The distance from the bottom of the chamber to the lower edge of the nozzles was varied within the range 0-70 mm. When we placed a symmetrical insert with a trapezoidal notch and a rectangular uniflow nozzle 32 mm wide into the lower part of the chamber, we changed the model over to the fountain-vortex design [7] depicted in Fig. 2. In this case, the distance between the inlet and the roof of the furnace was 510 mm. Profiles of velocity and the level of the turbulent pulsations were measured by the electrodiffusion method [8], while pressure was measured with a bank of differential manometers of the water type. The flow pattern was visualized by means of air bubbles. The setup of the experiment is described in more detail in [9]. The Reynolds number, determined from the width of the nozzle and the velocity at the inlet, was $3.3 \cdot 10^4$ for the rectangular chamber and $7.04 \cdot 10^4$ for the model with the fountain-vortex furnace.

Flow in the case of the above described furnace configurations includes circulation zones, sections of rapid change in direction, and other features that make it appropriate

TABLE 1. Conservation Equations Generated by Eq. (1)

Physical quantities	Φ	Γ_Φ	S_Φ
Mass	1	0	0
Momentum in the horizontal direction	U	μ_{ef}	$\frac{\partial}{\partial x}\left(\mu_{ef}\frac{\partial U}{\partial x}\right)+\frac{\partial}{\partial y}\left(\mu_{ef}\frac{\partial V}{\partial x}\right)-\frac{\partial P}{\partial x}$
Momentum in the vertical direction	V	μ_{ef}	$\frac{\partial}{\partial x}\left(\mu_{ef}\frac{\partial U}{\partial y}\right)+\frac{\partial}{\partial y}\left(\mu_{ef}\frac{\partial V}{\partial y}\right)-\frac{\partial P}{\partial y}$
Eddy kinetic energy	k	$\frac{\mu_{ef}}{\sigma_k}$	$G_k-\rho\varepsilon$
Rate of dissipation of turbulence energy	ε	$\frac{\mu_{ef}}{\sigma_\varepsilon}$	$\frac{\varepsilon}{k}(C_1G_k-C_2\rho\varepsilon)$

$$G_k=\mu_{ef}\left[2\left(\left(\frac{\partial U}{\partial x}\right)^2+\left(\frac{\partial V}{\partial y}\right)^2\right)+\left(\frac{\partial U}{\partial y}+\frac{\partial V}{\partial x}\right)^2\right].$$

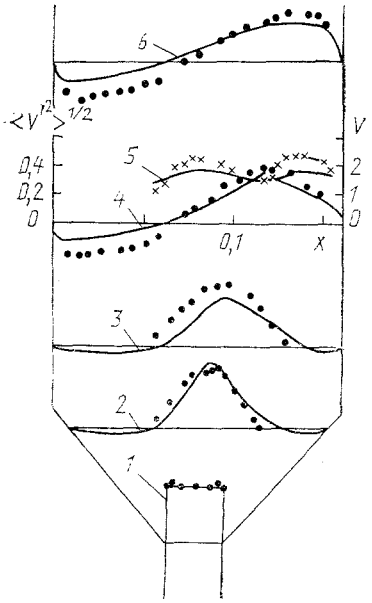

Fig. 2. Profiles of the averaged and fluctuational parts of vertical component of velocity in different sections of the fountain-vortex furnace model (curves — calculation; points — experiments): 1) V, y = 0 m; 2) V, y = 0.065; 3) V, y = 0.11; 4) V, y = 0.18; 5) $\langle V'^2\rangle^{1/2}$, y = 0.18; 6) V, y = 0.27. x, m; V, $\langle V'^2\rangle^{1/2}$, m/sec.

to use elliptic differential equations to describe the processes taking place in the chamber. Reduced to divergence form, the steady-state equations describing the incompressible flow can be written in generalized form

$$\frac{\partial}{\partial x}(\rho U\Phi)+\frac{\partial}{\partial y}(\rho V\Phi)=\frac{\partial}{\partial x}\left(\Gamma_\Phi\frac{\partial\Phi}{\partial x}\right)+\frac{\partial}{\partial y}\left(\Gamma_\Phi\frac{\partial\Phi}{\partial y}\right)+S_\Phi. \quad (1)$$

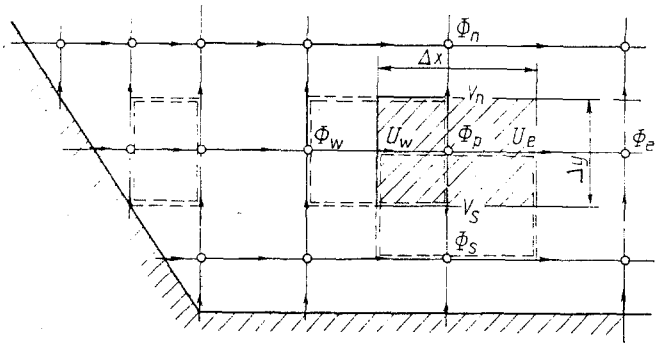

Fig. 3. Structure of the theoretical region.

Values Γ_Φ and S_Φ corresponding to different physical quantities Φ are shown in Table 1. The introduction of k–ε equations makes it possible to close the system of equations for the averaged flow. In accordance with the Kolmogorov hypothesis, $\mu_T = \rho C_\mu k^2/\varepsilon$. Effective viscosity is determined as $\mu_{ef} = \mu_T + \mu$. We used the turbulence-model constants recommended by Rodi [10] $C_\mu = 0.09$; $C_1 = 1.44$; $C_2 = 1.92$; $\sigma_k = 1.0$; $\sigma_\varepsilon = 1.3$.

The first step in the solution of Eqs. (1) is to discretize the theoretical region. We use control-volume method [11], which is a variant of method of weighted errors. To obtain a discrete analog of the given differential equation in this method, the region is subdivided into non-intersecting elements (control volumes). Each such element contains one node of the grid. An important property of the control-volume method is satisfaction of the conservation laws for the physical quantities for any set of control volumes. Thus, even the solutions obtained on relatively coarse grids by this method satisfy the integral conservation conditions.

Another important aspect of the problem is the method used to arrange the nodes of the grid. Several of the difficulties normally encountered in the calculation of aerodynamic fields can be overcome by using the mixed or "staggered" grid introduced in [12]. A distinguishing feature of this grid is that the nodes at which the components of the velocity vector are determined are displaced a half-step in the corresponding velocity directions relative to the nodes used for all scalar quantities.

All of the control volumes are constructed on the basis of the same principle: the boundaries for the scalars pass through the nodes for the velocity components. This can be seen from Fig. 3, which shows the control volumes for the velocities. To facilitate performing calculations for flows within a broad range of characteristic scales, we used a nonuniform grid.

In accordance with the principle of the constancy of the physical quantities at the boundaries [11], by integrating Eq. (1) over the control volume we obtain

$$\Delta y\left(\rho U\Phi - \Gamma_\Phi \frac{\partial \Phi}{\partial x}\right)_e - \Delta y\left(\rho U\Phi - \Gamma_\Phi \frac{\partial \Phi}{\partial x}\right)_w \tag{2}$$

$$+ \Delta x\left(\rho V\Phi - \Gamma_\Phi \frac{\partial \Phi}{\partial y}\right)_n - \Delta x\left(\rho V\Phi - \Gamma_\Phi \frac{\partial \Phi}{\partial y}\right)_s = S_\Phi \,\mathrm{vol}_\Phi.$$

When Eq. (2) is changed to discrete form, it is necessary to make certain additional assumptions on the character of the change in the quantities being investigated. In the present study, we use an exponential interpolation profile [11].

The main idea behind the algorithm SIMPLE [13], used here to determine the pressure field, is the introduction of corrections to pressure in each iteration. The use of these corrections makes it possible to satisfy the continuity equation. The velocity field is refined on the basis of the corrections that are calculated.

Boundary conditions at the inlet were assigned in the form of uniform profiles. The eddy kinetic energy k_{in} and rate of dissipation ε_{in} were expressed through the velocity at the inlet and the width of the slotted nozzle L in the following manner: $k_{in} = 0.01U_{in}^2$;

$\varepsilon_{in} = k_{in}^{3/2}/L$.

The "mild" boundary condition $\partial^2\Phi/\partial x^2 = 0$ was assigned for all quantities at the outlet.

The transverse component of velocity was taken equal to zero at both the inlet and outlet.

Boundary functions were used to determine the characteristics of the flow near the boundaries. Without reducing the accuracy of the calculations, the introduction of boundary functions to account for the behavior of aerodynamic fields in the boundary layer makes it possible to place the grid node that is closest to the boundary at a certain distance from the wall. As an example, we will examine the realization of boundary conditions on the horizontal (lower) wall.

The method is based on the assumption that eddy kinetic energy does not change across the logarithmic layer:

$$k = U_*^2/C_\mu^{1/2}. \tag{3}$$

The following relation is valid for the rate of dissipation

$$\varepsilon = U_*^3/\varkappa y, \tag{4}$$

this relation corresponding to the following velocity profile:

$$U = \frac{U_*}{\varkappa} \ln (Ey_+), \tag{5}$$

where $y+ = yU*/\nu$; E is a constant dependent on the roughness of the wall (we take $E = 7.7$, $\kappa = 0.4$).

Now, determining the following in terms of k

$$y_+ = \frac{C_\mu^{1/4} k^{1/2} y}{\nu},$$

we obtain the relations:

$$\tau = -\frac{C_\mu^{1/4} \varkappa \rho k^{1/2} U}{\ln (Ey_+)}, \tag{6}$$

$$\varepsilon = \frac{C_\mu^{3/4} k^{3/2}}{\varkappa y}. \tag{7}$$

Condition (6) is used to close the equation for the longitudinal component of velocity, while condition (7) directly determines the rate of dissipation at the first node. We calculate the term which accounts for dissipation at the boundary node by integrating the expression for ε over the region of the control volume outside the viscous sublayer. We find the mean rate of generation of turbulence energy as $|\tau U|/y$.

The condition of the absence of flow V = 0 (Fig. 3) is used for the transverse component of velocity.

In the general case, the boundaries of the theoretical region may be located at an arbitrary angle to the grid lines. There are no descriptions in the literature of a regular method of accounting for oblique boundaries on a "staggered" grid. Most investigators circumvent this problem by replacing such boundaries by stepped boundaries [4-6]. However, this results either in a significant reduction in accuracy due to induced flow separation or in an intolerably large increase in the number of grid nodes. A method of allowing for oblique

boundaries was devised to eliminate these shortcomings. The grid is constructed in such a way that all of the walls intersect the boundaries of the cells of the main grid halfway between the nodes. This is shown in Fig. 3 for the left lower sloping wall. Only one croner of the control volumes for the velocity components touches the sloping walls, which makes it possible to use the standard procedure described above for the internal nodes. It is assumed that the flow is nearly parallel to the wall where it is near to it. Replacing U in Eq. (5) by the total velocity, we find the value of flow velocity U_* iteratively. Then we use (3-4) to determine kinetic energy and rate of dissipation at the nodes adjacent to the inclined boundaries.

We will use the method of line relaxation to obtain a numerical solution to the equations with the above-formulated boundary conditions. This method makes it possible to invert the matrices of the equations by using an iterative procedure consisting of two cycles. In the external cycle, we choose a set of nodes lying on one line such that one of the indices coincides for all of these nodes. The values of the variables at the remaining nodes are fixed. In the internal cycle, we calculate the values at the nodes on the line. Here, we use a standard method to invert the tridiagonal matrices (trial-run method).

Numerical calculations showed that the most rapid convergence is obtained if the direction of the trial run is chosen to be orthogonal to the streamlines. In accordance with this finding, we subdivided the region into several zones with different methods of cycle organization. It should be mentioned that these zones were allowed to overlap.

The lower relaxation coefficients for all of the equations depends heavily on the character of the flow. However, their value is generally no greater than 0.6 for velocity and 0.4 for the $k-\varepsilon$ equations.

Systematic calculations were performed on 30 × 60 grids for a rectangular furnace chamber and 40 × 60 grids for the fountain-vortex model.

Two different types of flows are realized in the case of unilateral delivery of the fluid (see Fig. 1a and b). At small distances H from the lower edge of the nozzle to the bottom of the chamber, ejection of the jet creates a zone of reduced pressure between the jet and the lower surface. The presence of a rarefaction region causes the jet to be drawn out toward the bottom (Fig. 1a). The phenomenon of the "sticking" of a jet to walls is known as the Koand effect and generally has an adverse effect on heat-transfer and combustion. The attached jet subsequently develops as a wall jet which propagates along the furnace baffles. Two vortical zones are formed. One occupies most of the furnace chamber. The other zone, located below the nozzle, is bounded by the right wall and the point of attachment of the jet.

The position of the point of attachment of the jet determined from the calculations depends to a considerable extent on the mesh of the grid. For steady-state flows, two groups of errors caused by the theoretical scheme can be distinguished. The first consists of so-called "one-dimensional" errors, which are minimal in the case of the power-law scheme being employed here. The second group includes numerical errors caused by the noncoincidence of the orientations of the streamlines with the lines of the grid. The size of this type of error is proportional to the velocity averaged over the control volume and increases with an increase in the dimensions of the cells of the grid [14].

The given flow is characterized by a high degree of inertia in the plane jet. Its momentum is thus conserved and, consequently, so is velocity at large distances from the inlet. To determine the extent of the effect of numerical diffusion, associated with the second type of error mentioned above, we performed a series of calculations on a set of grids of increasing density. Attachment was delayed as the mesh of the grid was reduced. However, with a substantial increase in the number of nodes along the vertical (up to 30), attachment in the lower region of the chamber occurred somewhat earlier than in the experiment. The phenomenon of premature attachment of the jet due to the use of the $k-\varepsilon$ model was mentioned in [15].

With movement of the bottom in the downward direction, the point of attachment shifts to the left and, as shown by the calculations, suddenly moves to the opposite wall at H = 50 mm (Fig. 1b). This is accompanied by an increase in the size of the lower recirculation region.

Figure 4 shows the pressure distribution over the bottom of the channel P relative to the pressure taken as the "zero" value — the pressure at the lower edge of the nozzle. The

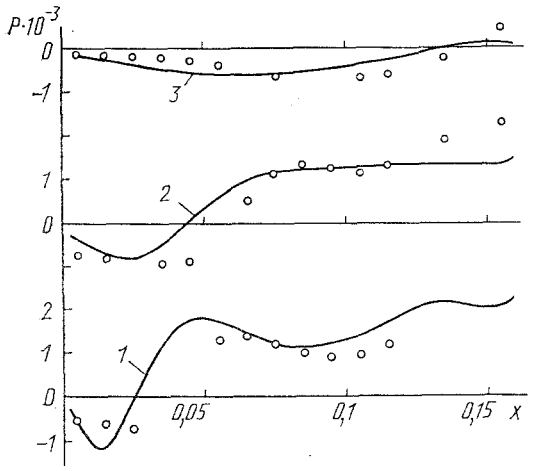

Fig. 4. Distribution of bottom pressure in a rectangular channel with different distances from the bottom to the lower edge of the nozzle (the curves show calculated results, while the points show experimental data): 1) H = 0.02 m; 2) 0.029; 3) 0.065. P, Pa.

curves show the results of the variant calculations. The longitudinal coordinate x was reckoned from the wall on which the nozzle was located.

We obtained satisfactory agreement between the calculations and the experiment. The local pressure peak seen for the cases H = 20, 29 mm is connected with attachment of the jet near the middle of the bottom. Thus, the peak is absent for the case H = 65 mm. On the whole, the character of the distribution of bottom pressure agrees with the data obtained by other investigators. The typical result obtained with the use of the $k-\varepsilon$ model [15] is the occurrence of a larger pressure gradient in the vortical region in the regimes in which attachment takes place. The deviation of the pressure field from the experimental value near the boundaries is evidently due to the ineffectiveness of the boundary-functions method at flow rotation points.

In the case of bilateral delivery, the interaction of the counter-directed jets leads to a change in the character of the flow compared to unilateral delivery. As an example, Fig. 1c shows the streamlines which are present at H = 30 mm. Nonsteady two-dimensional flow with transverse deviations of the jets in the vertical direction were seen in [9] in experiments conducted with large H. When the slotted nozzle is replaced by nozzle with circular holes simulating burners, large-scale pulsations are suppressed. The transition from one flow regime to the other with a change in the inlet conditions is due to the presence, in the latter case, of regions around the burners where intensive mixing is taking place. It should be noted that Eqs. (1) actually describe quantities that are averaged over the depth of the furnace chamber. As regards the diffusion coefficients Γ_Φ of the averaged quantites, they include both turbulent transport and dispersive transport [10], which occurs due to the nonuniformity of the velocity distribution in the depth direction. In particular, this distribution is step-like in character along the burner belt. While most of the change in the diffusion characteristics which is due to dispersion can be ignored, its effect at the inlet will be substantial. The effect of dispersive transport, concentrated in the region where the turbulent jets issuing from the burners are mixed, leads to an increase in turbulence energy and, thus, to the damping of large-scale pulsations. In practice, it is necessary to introduce an effective diffusion coefficent. This coefficient is chosen either on the basis of analysis of empirical data or by modeling processes in the mixing region.

Figure 2 shows the flow pattern which develops in the fountain-vortex model. The outlet section of the model (not shown) is located to the right. After leaving the nozzle, the jet attaches itself to the right wall. A relatively small circulation zone is located near the lower part of this wall. A second circulation zone is located near the left wall and occupies more than two-thirds of the volume of the chamber. It begins at the left edge of the nozzle and ends on the top wall of the model. In the experiment, attachment of the jet oc-

curred with equal probability on the right and left walls and was determined by the initial conditions of the experiment. Qualitative agreement between the experimental and theoretical velocity profiles was seen in all sections. However, quantitative agreement was not seen everywhere. The theoretical values tended to deviate from the experimental data in the upper circulation zone. On the whole, the theoretical velocity fields show a more viscous flow than does the experiment. However, the differences between the two sets of values lies within the experimental error almost everywhere. One reason for the quantitative difference between the experimental and theoretical results might be that the flows in the model were to a certain extent three-dimensional. The velocity distributions shown in Fig. 2 correspond to a section located the same distance from the front and rear walls of the model. Due to the effect of these walls, the velocity distribution in the direction perpendicular to the plane of the figure is not completely uniform. The velocity maximum is apparently located in the section shown in the figure. This effect was not taken into account in the two-dimensional calculation. With respect to the fluctuation component of velocity, the agreement between theory and experiment turned out to be somewhat better than the agreement for the averaged component. The distributions in the section located 0.18 m from the inlet are shown as an example.

The above comparison with experimental results illustrates the efficiency of the proposed application package to describe turbulent flows in furnace chambers. It also shows that a standard turbulence model with the above-examined boundary-functions model can be used in the computations, along with an algorithm that accounts for the presence of boundaries that are not orthogonal to a "staggered" grid.

NOTATION

x, y, cartesian coordinates; U, V, corresponding components of the vector of averaged velocity; ρ, density; Φ, Γ_Φ, S_Φ, generalized coefficient and the transport coefficient and source term corresponding to it in the conservation equation; k, eddy kinetic energy; ε, rate of dissipation; G_k, rate of generation; μ_T, M_{ef}, dynamic turbulence coefficient and effective viscosity coefficient; C_μ, C_1, C_2, G_k, σ_ε, constants of the turbulence model; L, width of nozzle; U_*, flow velocity; χ, von Kármán constant; ν, kinematic viscosity; τ, shear stresses on the wall; H, distance from the lower edge of the nozzle to the bottom; P, pressure; F, stream functional normalized with respect to total discharge; $\langle V'^2 \rangle^{1/2}$, root-mean-square value of velocity fluctuations in the vertical direction; vol_Φ, area of control volume. Indices: n, s, e, w determine the orientation of the nodes relative to the specified node p; in, for quantities being examined at the inlet.

LITERATURE CITED

1. V. K. Migai, Modeling Heat-Exchangers in Power Plants, Leningrad (1987).
2. B. P. Ustimenko, K. B. Dzhakupov, and V. O. Krol', Numerical Modeling of Aerodynamics and Combustion in Furnaces and Process Equipment [in Russian], Alma-Ata (1986).
3. F. C. Lockwood, C. Papadopoulos, and A. S. Abbas, Combust. Sci. Technol., 58, 5-23 (1988).
4. W. A. Fiveland and R. A. Wessel, J. Eng. Gas Turb. Power, 110, No. 1, 117-126 (1988).
5. K. Gorner and W. Zinser, Combust. Sci. Technol., 58, 43-57 (1988).
6. V. Vrublevska, A. Vanik, and E. Shimchak, Teploenérgetika, No. 10, 69-72 (1987).
7. Furnace: Inventor's Certificate No. 1239452 SSSR, MKI⁴ F 23 C 5/08.
8. V. E. Nakoryakov, A. P. Burdukov, O. N. Kashinskii, and P. I. Geshev, Electrodiffusion Method of Studying the Local Structure of Turbulent Flows [in Russian], Novosibirsk (1986).
9. S. V. Alekseenko, M. Ya. Protsailo, and A. V. Yurlagin, Izv. Sib. Otd. Akad. Nauk SSSR, Ser. Tekh. Nauk, 2, No. 7, 34-38 (1988).
10. V. Rodi, in: Methods of Calculating Turbulent Flows [Russian translation], Moscow (1984), pp. 227-322.
11. S. Patankar, in: Numerical Methods of Solving Problems of Heat Transfer and Fluid Dynamics [Russian translation], Moscow (1984).
12. F. H. Harlow and J. E. Welch, Phys. Fluids, 8, No. 12, 2182-2189 (1965).
13. S. V. Patankar and D. B. Spalding, Int. J. Heat Mass Transfer, 15, No. 10, pp. 1787-1806 (1972).
14. M. A. Leschzinger, Comp. Meth. Appl. Mech. Eng., 23, No. 3, 293-312 (1980).
15. M. Nallasamy, Comput. Fluids, 15, No. 2, 151-194 (1987).